

**Christoph Mueller-Dieckmann,^{a*}
 Stefan Kernstock,^b Jochen
 Mueller-Dieckmann,^c Manfred S.
 Weiss^c and Friedrich Koch-
 Nolte^b**

^aESRF, 6 Rue Jules Horowitz, F-38043 Grenoble
 CEDEX 09, France, ^bInstitute of Immunology,
 University Hospital, Martinistrasse 52,
 D-20246 Hamburg, Germany, and ^cEMBL
 Hamburg Outstation, c/o DESY,
 Notkestrasse 85, D-22603 Hamburg, Germany

Correspondence e-mail: muellerd@esrf.fr

Received 13 December 2007

Accepted 14 January 2008

PDB Reference: ADP-ribosylhydrolase 3, 2qtj,
 r2qtsf.

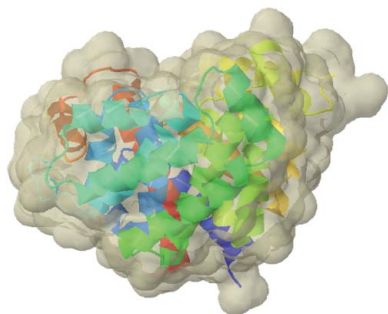
Structure of mouse ADP-ribosylhydrolase 3 (mARH3)

ADP-ribosylation is a reversible and covalent post-translational modification in which the attachment of ADP-ribose is catalyzed by ADP-ribosyltransferases and the removal of ADP-ribose is catalyzed by ADP-ribosylhydrolases. ADP-ribosylhydrolase 3 from mouse, consisting of 347 amino-acid residues, has been cloned, purified and crystallized. The three-dimensional structure has been resolved at a resolution of 1.8 Å. The structure constitutes a compact all- α -helical protein with two Mg²⁺ ions located in the active-site crevice. A structural comparison of mouse ADP-ribosylhydrolase 3 with its human orthologue shows a high degree of structural similarity. Furthermore, four prokaryotic proteins deposited in the PDB could be identified as being structurally related.

1. Introduction

The addition of ADP-ribose onto proteins is a reversible post-translational modification that is catalysed by a variety of enzymes (Shall, 1995). It can occur either in the form of mono-ADP-ribosylation (Seman *et al.*, 2004) or in the form of poly-ADP-ribosylation (Hassa *et al.*, 2006). ADP-ribosylation is the reaction in which the ADP-ribose moiety of NAD is transferred to a specific acceptor amino-acid residue such as Arg, Asn, Glu, Asp, Cys, diphthamide or phosphoserine. During the stereospecific chemical reaction, the target performs a nucleophilic attack on the anomeric C atom of the ribose moiety adjacent to nicotinamide in NAD, thereby generating a covalent linkage with ADP-ribose and releasing nicotinamide. The hydrolysis of NAD itself can be described as a transfer of ADP-ribose onto a water molecule.

Many of the bacterial mono-ADP-ribosyltransferases (mARTs) are known for their toxicity. Prominent examples are diphtheria toxin, cholera toxin, *Salmonella* virulence factor SpvB and many others (Aktories & Just, 2000). ADP-ribosylating toxins catalyse the transfer of the ADP-ribose moiety from NAD to specific target proteins, in many cases GTP-binding or ATP-binding proteins. ADP-ribosylation often alters the function of the target protein and disrupts cellular metabolism. SpvB-related mammalian ecto-mARTs occur as glycosylphosphatidylinositol-anchored or secretory proteins that can be divided into five paralogues: mART1–5 (Glowacki *et al.*, 2002; Seman *et al.*, 2004). Diphtheria-toxin-related poly-ADP-ribosyltransferases or poly-(ADP-ribose) polymerases (pARTs or PARPs) are intracellular, usually nuclear, proteins of eukaryotes (Otto *et al.*, 2005; Schreiber *et al.*, 2006) that play a role in DNA repair (Malanga & Althaus, 2005), transcriptional activation and repression (Kim *et al.*, 2004), chromatin insulation (Yu *et al.*, 2004), cell death (Jagtap & Szabo, 2005), regulation of mitosis (Chang *et al.*, 2004) or the regulation of telomere length (Smith *et al.*, 1998). It has been suggested that some members of the mART and PARP families can act both as a mART and as a PARP (Otto *et al.*, 2005; Hassa *et al.*, 2006; Morrison *et al.*, 2006). Additionally, there is evidence for intracellular ADP-ribosylation, which may be catalyzed by certain members of the structurally distinct sirtuin family. For instance, SIRT4 has been shown to regulate insulin secretion by mono-ADP-ribosylating glutamate dehydrogenase (Haigis *et al.*, 2006; Ahuja *et al.*, 2007).



The extent and duration of mono-ADP-ribosylation depends on the activity of ADP-ribosylhydrolases (ARHs) and poly-ADP-ribosylglycohydrolases (PARGs), which reverse the transfer reaction by hydrolysing the protein-ADP-ribose bond and/or ADP-ribose-ADP-ribose bonds (Koch-Nolte & Haag, 1997; Moss *et al.*, 1997). In this context, mARTs/PARPs and ARHs/PARGs form opposite pairs in the ADP-ribosylation reaction cycle (Fig. 1). To date, three mammalian ARHs (ARH1–3) have been described (Glowacki *et al.*, 2002), where ARH1 has been reported to cleave ADP-ribosyl-arginine (Moss *et al.*, 1997) and ARH3 to de-ADP-ribosylate poly-ADP-ribosylated proteins (Oka *et al.*, 2006; Mueller-Dieckmann *et al.*, 2006) and to hydrolyse *O*-acetyl-ADP-ribose (Ono *et al.*, 2006). ARH3 localizes to the mitochondrial matrix, where it can efficiently degrade poly-ADP-ribose generated by mitochondrially targeted PARP1 in living cells (Niere *et al.*, 2008). PARG is encoded by a single-copy gene in mammals, which is transcribed into different splice variants that mediate differential subcellular localization to the nucleus, cytosol and mitochondria (Meyer *et al.*, 2007). PARG cleaves ADP-ribosyl-ADP-ribose linkages but is not known to cleave ADP-ribosyl-amino-acid linkages.

The only structurally characterized member of the ARH and PARG protein families is human ARH3 (Kernstock *et al.*, 2006; Mueller-Dieckmann *et al.*, 2006). The crystal structure of human ARH3 revealed two Mg²⁺ ions to be localized in the active-site crevice. Since these are essential for the full activity of the protein, which has been demonstrated for the related enzyme ARH1 (Moss *et al.*, 1985), they pinpoint the active site. Binding of ADP-ribose to human ARH3 has been confirmed by isothermal titration microcalorimetry experiments and the binding mode was evaluated by docking studies (Mueller-Dieckmann *et al.*, 2006). Site-directed mutagenesis of amino-acid residues predicted to be involved in binding ADP-ribose and/or the magnesium ions resulted in a severe loss of enzymatic activity, supporting the suggested binding mode (Mueller-Dieckmann *et al.*, 2006).

Mouse ARH3 (ADPRHL2) consists of 370 amino acids and shares 17 and 16% amino-acid sequence identity with the mouse paralogues ARH1 and ARH2, respectively, and 90% identity with the human orthologue. Here, we present the structure of ARH3 from *Mus musculus* refined to a resolution of 1.8 Å and a comparison with its human orthologue and with other structurally related proteins.

2. Materials and methods

2.1. Cloning, expression and purification

A cDNA clone encompassing the coding region for mARH3 was obtained from the IMAGE consortium (IMAGE Consortium Clone ID 5293159; Lennon *et al.*, 1996). The ARH coding region excluding a putative N-mitochondrial targeting sequence (residues 2–23) was amplified by PCR with appropriate primers (5'-CGATGACCA-TATGCGCTCCATCTCGCGCTTCG-3' and 5'-AAGCACTCGA-GCGAGCTCTCCTGGAAGACTCGGT-3') and cloned into the *Nde*I and *Xho*I sites of the prokaryotic expression plasmid pET26b (Novagen). This cloning strategy resulted in the removal of the pelB leader sequence from pET26b, the deletion of residues 2–23 of mARH3 and a C-terminal extension of two amino acids encoded by the *Xho*I recognition sequence (Leu-Glu) followed by a hexahistidine tag. The correct cloning of the gene was verified by DNA sequencing.

The expression plasmid pET26b-mARH3 was freshly transformed into *Escherichia coli* BL21-CodonPlus(DE3)-RIL cells (Stratagene). A single colony was picked for an overnight preculture, which took

place at 310 K in LB broth medium containing 50 µg ml⁻¹ kanamycin and 30 µg ml⁻¹ chloramphenicol. 5–10 ml of this preculture was used to inoculate a 1 l culture, which was grown at 310 K to an optical density at 600 nm (OD₆₀₀) of approximately 0.5. The temperature was then reduced to 293 K and expression was induced by adding isopropyl β-D-thiogalactopyranoside (IPTG) to a final concentration of 1 mM when an OD₆₀₀ of about 0.7 was reached. After induction, cells were grown for an additional 15 h and harvested. The cells were then frozen at 253 K until further processing.

1 g of the cells was suspended in 4 ml lysis buffer [50 mM Tris pH 8.0, 150 mM NaCl, 3 mM β-mercaptoethanol (β-ME), 10 mM MgCl₂ and 0.1% (v/v) Triton X-100]. After lysis by sonication, the cell debris was removed by centrifugation at 20 000 rev min⁻¹ at 277 K for 30 min. The clear supernatant was passed onto a Ni-NTA Superflow column (Qiagen) that had been equilibrated with lysis buffer. After extensive washing (ten column volumes) with washing buffer (50 mM Tris pH 8.0, 300 mM NaCl, 3 mM β-ME and 5 mM MgCl₂), the protein was eluted in a buffer containing 50 mM Tris pH 8.0, 300 mM NaCl, 3 mM β-ME, 5 mM MgCl₂ and 500 mM imidazole. The eluate was concentrated to a volume of less than 1 ml and directly applied onto a Sephacryl-S200 size-exclusion column (Amersham Pharmacia). mARH3 eluted in a buffer containing 50 mM Tris pH 8.0, 150 mM NaCl and 2 mM DTT with a molecular weight of about 40 000 Da, corresponding to a monomer in solution. Protein-containing fractions exhibiting a purity of higher than 95% were pooled, concentrated and dialyzed extensively against 10 mM HEPES pH 7.0 and 150 mM NaCl. Typical yields were around 15 mg of pure protein per litre of culture.

2.2. Crystallization

Prior to crystallization, the protein concentration was adjusted to 5 mg ml⁻¹. Initial screening for crystals was performed at the High-Throughput Crystallization facility of the EMBL Outstation in Hamburg (Mueller-Dieckmann, 2006). The sample was tested in five commercial initial screens (Crystal Screens I and II, Index and SaltRx from Hampton Research and Jena 1–8 from Jena Bioscience). In the refined crystallization conditions, crystals were grown at 295 K, mixing protein and reservoir solution [100 mM MES pH 6.2 and 6% (w/v) PEG 4000] in a 1:1 ratio. Crystals appeared within one to two weeks as long needles that were often badly grown together (up to 1 mm in length and 150 µm in width; Fig. 2).

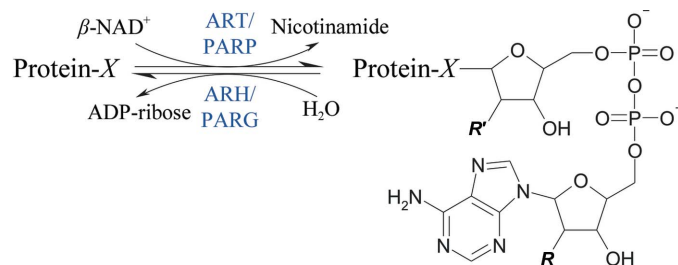


Figure 1

The reversible ADP-ribosylation reaction. ARTs and PARPs catalyse the transfer of an ADP-ribose moiety from NAD onto specific amino-acid residues or onto ADP-ribose, respectively, thereby releasing nicotinamide. The reverse reaction is catalysed by ARHs or PARGs through the hydrolysis of the α-glycosidic bond between ADP-ribose and the side chain. *X* can be Arg, Asp, Glu, Asn, Cys, diphthamide or ADP-ribose. For mono-ADP-ribosylation *R* and *R'* are hydroxyl groups, while for poly-ADP-ribosylation ADP-ribose can be attached to the *R* site (elongation) or to the *R'* site (branching).

2.3. Structure determination and refinement

Prior to diffraction data collection, a crystal of mARH3 was cryoprotected by soaking it in 20% (v/v) glycerol in reservoir solution for 20 s and then flash-cooled in a 100 K nitrogen stream. Diffraction data were then collected to a diffraction limit of 1.8 Å (Table 1) at EMBL beamline X11 (DESY Hamburg, Germany) using a MAR CCD (165 mm) detector. The data were indexed, integrated and scaled using *DENZO* and *SCALEPACK* (Otwinowski & Minor, 1997). Intensities were converted to structure-factor amplitudes using the program *TRUNCATE* (French & Wilson, 1978; Collaborative Computational Project, Number 4, 1994). Initial phases were obtained by molecular replacement with the program *MOLREP* (Vagin & Teplyakov, 1997; Collaborative Computational Project, Number 4, 1994) using the human orthologue (Mueller-Dieckmann *et al.*, 2006) as a search model (PDB code 2foz). After having correctly oriented and placed both molecules in the asymmetric unit, the model amino-acid sequence was modified to reflect the sequence of mouse ARH3 using the program *Coot* (Emsley & Cowtan, 2004; Colla-



Figure 2 Crystal of mARH3. The bar in the upper right corner corresponds to 100 µm.

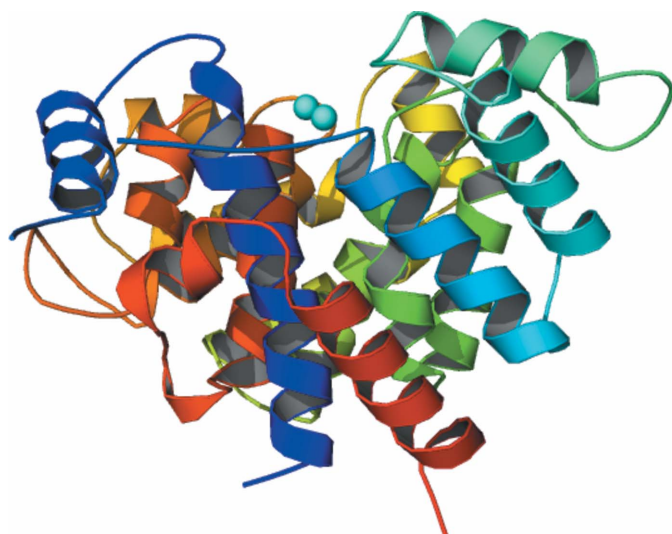


Figure 3 Ribbon-plot representation of mARH3. The colouring scheme is from the N-terminus (blue) to the C-terminus (red). It is identical to that chosen for the human orthologue (Mueller-Dieckmann *et al.*, 2006) for better comparison. The two magnesium ions in the active-site crevice are shown as cyan spheres. The ill-defined loop between α -helices 2 (dark blue) and 3 (light blue) has not been drawn in the representation.

Table 1 Data-collection and processing statistics.

Data-collection wavelength	0.8126
Space group	$P2_1$
Unit-cell parameters	
a (Å)	53.88
b (Å)	60.10
c (Å)	91.78
β (°)	90.09
Resolution limits (Å)	99–1.80 (1.83–1.80)
Mosaicity (°)	1.0
Total no. of reflections	345718
No. of unique reflections	51153
Redundancy	6.8 (6.5)
$\langle I/\sigma(I) \rangle$	23.9 (2.5)
Completeness	93.8 (89.2)
$R_{\text{merge}}^{\dagger}$ (%)	7.7 (80.3)
$R_{\text{r.i.m.}}^{\ddagger}$ (%)	8.3 (87.0)
$R_{\text{p.i.m.}}^{\ddagger}$ (%)	3.1 (32.9)
Optical resolution (Å)	1.49
Overall B factor from Wilson plot (Å ²)	24.8

$\dagger R_{\text{merge}}(I) = \frac{\sum_{hkl} \sum_i |I_i(hkl) - \langle I(hkl) \rangle|}{\sum_{hkl} \sum_i I_i(hkl)}$. \ddagger The redundancy-independent merging R factor ($R_{\text{r.i.m.}} = \frac{\sum_{hkl} [N/(N-1)]^{1/2} \sum_i |I_i(hkl) - \langle I(hkl) \rangle|}{\sum_{hkl} \sum_i I_i(hkl)}$) and the precision-indicating merging R factor ($R_{\text{p.i.m.}} = \frac{\sum_{hkl} [1/(N-1)]^{1/2} \sum_i |I_i(hkl) - \langle I(hkl) \rangle|}{\sum_{hkl} \sum_i I_i(hkl)}$) (Weiss, 2001) were calculated using the program *RMERGE* (available from MSW upon request or from http://www.embl-hamburg.de/~msweiss/projects/msw_qual.html).

Table 2 Refinement statistics.

Refinement	
Resolution limits (Å)	30–1.80
No. of reflections	
Working set	50111
Test set	975
R_{cryst} (%)	16.7
R_{free} (%)	19.8
No. of atoms	
Protein	5181
Ions	4
Waters	200
Stereochemistry	
R.m.s. deviations	
Bonds (Å)	0.016
Angles (°)	1.47
Average B factors (Å ²)	
Protein	18.3
Ions	12.5
Waters	19.6
Ramachandran plot	
Most favoured (%)	97.0
Allowed (%)	2.4

borative Computational Project, Number 4, 1994). Refinement was performed using the program *REFMAC5* (Winn *et al.*, 2001; Collaborative Computational Project, Number 4, 1994). Refinement statistics are summarized in Table 2.

3. Results and discussion

3.1. Overall structure

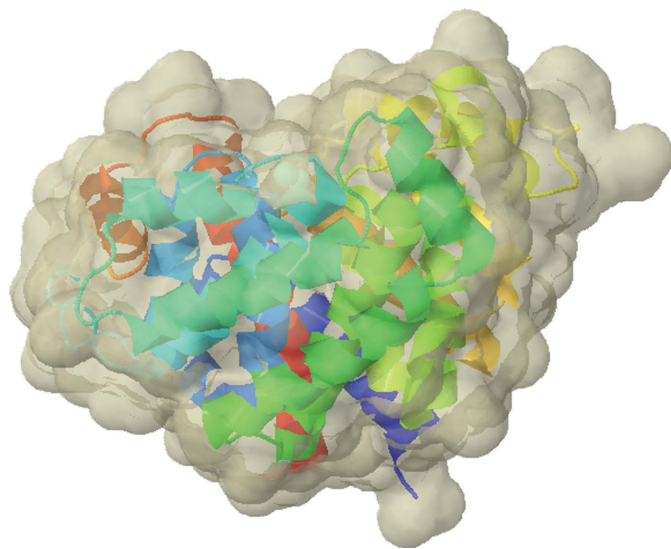
The complete model consists of 674 amino acids in two protomers, four Mg^{2+} ions and 200 water molecules. Although the content of the asymmetric unit of the crystal is two protomers, the most likely biological unit is a monomer, as also evidenced by size-exclusion chromatography, which indicates that the protein is monomeric in solution. Both all- α -helical protomers are composed of 19 α -helices, with two Mg^{2+} ions that pinpoint the active-site crevice, and have dimensions of approximately $53 \times 50 \times 62 \text{ \AA}^3$ (Fig. 3 and Fig. 4). The first 23 N-terminal amino-acid residues, *i.e.* the predicted mitochondrial targeting sequence, have been replaced by a Met residue during

Table 3Coordination of the two Mg²⁺ ions.

Bridging atoms are highlighted in bold. Mean distances from structures in the PDB at near-atomic resolution are 2.09 Å for Mg²⁺–OH₂, 2.10 Å for Mg²⁺–O Thr, 2.08 Å for monodentate Mg²⁺–[−]OOC Asp/Glu and 2.5 Å as the maximal accepted distance of bidentate Mg²⁺–[−]OOC Asp/Glu (Harding, 2001, 2006). The two coordinating atoms of the Mg-II ion that differ by more than 50% from the mean distance are indicated in italics. Values for the deviation of the mean distance assuming a bidentate coordinating nature are given in parentheses.

Coordinating atom	Distance (Å)	Deviation from mean distance (%)
Mg-I		
Thr60 OG1	2.32	+10.5
Asp61 OD1	2.03	−2.4
Asp62 OD2	1.93	−7.2
Asp300 OD2	2.01	−3.4 (19.6)
W20	2.10	+0.5
W61	2.02	−3.3
Mg-II		
Glu25 OE2	2.26	+8.7
Asp298 OD1	2.17	+4.3 (13.2)
<i>Asp298 OD2</i>	<i>3.42</i>	<i>+64.4 (36.8)</i>
Asp300 OD1	2.20	+5.8 (12.0)
Asp300 OD2	3.16	+51.2 (26.4)
Thr301 OG1	2.32	+10.5
W38	2.27	+8.6
W61	2.23	+6.7

cloning. The loop regions from Asp45 to Thr54 in both protomers *A* and *B* as well as the two C-terminal serine residues and the subsequent His₆ tag are missing from the model owing to ill-defined electron density. The two protomers in the asymmetric unit exhibit an average r.m.s. deviation of only 0.69 Å for all 335 superimposed C^α positions. A comparison of the *B*-factor distribution with the difference of C^α positions in both protomers shows that the regions exhibiting higher *B* factors generally also exhibit the highest C^α discrepancies. The four internal loop regions are (i) the ‘missing’ loop (residues 45–54), (ii) the loop region between α-helices 10 and 11 (residues 188–192), which is situated at the crystal contact between the two protomers, (iii) the loop region between α-helices 12 and 13 (residues 218–224), which is also on the surface, and (iv) the loop

**Figure 4**

Ribbon-plot representation and protein solvent-accessible surface representation. The colouring scheme for the protein chain is from the N-terminus (blue) to the C-terminus (red). The solvent-accessible surface is coloured grey and the two Mg²⁺ ions are shown as cyan spheres.

Table 4

Amino-acid substitutions between mouse and human ARH3.

Conservative substitutions are marked with an asterisk after the amino-acid position.

Amino-acid position	Amino acid in mARH3	Amino acid in hARH3	Comment
4*	Ile	Leu	
22*	Ala	Ser	6.6 Å from Mg
23*	Val	Phe	
31	Ser	Asp	
33*	Ala	Thr	
37	Ser	Arg	
40*	Glu _A	Gln	Salt bridge to Arg _B 117 (sym)
52	Ala	Glu	
56*	Thr	Ala	
66*	Thr	Ala	Located in protein core
105*	Ile	Val	
120*	Tyr _B	Phe	Hydrogen bond to Glu _B 81
189	Val	Glu	
197	Glu	Lys	
205*	Glu	Asp	
217*	Lys	Arg	
233*	Val	Ile	Located in protein core
240	Asp	Ala	
241	Val	Ser	
243*	Ser _A	Thr	Hydrogen bond to Glu _A 245
	Ser _B	Thr	Hydrogen bond to Glu _B 246
275	His	Asp	
281*	Thr	Ala	
317*	Glu	Asp	
330*	Phe	Tyr	
335*	Val	Ile	
346	Glu _B	Lys	Hydrogen bond to His _B 341

between α-helices 15 and 16 (residues 271–283), which like (ii) can be found at the crystal contact of the two protomers.

3.2. Active site

The chain termini are situated close to each other on the same side of the molecule. Two Mg²⁺ ions are located at the opposite side of the molecule within a cleft that spans nearly the entire width of the molecule. These metal ions are separated from each other by 3.74 Å and pinpoint the active site in which the ADP-ribose polymer is hydrolysed. The four tightly bound ions (two per protomer) show an average *B* factor of 12.5 Å², which is lower than the average *B* factor for the protein itself (18.3 Å²) and explains why Mg²⁺ ions did not have to be present during size-exclusion chromatography and crystallization. Each of the Mg²⁺ ions is nearly perfectly octahedrally coordinated by three and five acidic residues (Glu and Asp), respectively, one Thr residue and two water molecules. The corresponding residues, distances and deviation from ideal geometry are listed in Table 3. While the distances to the coordinating atoms for the first Mg²⁺ ion deviate on average just 4.5% from ideal distances, the deviation from ideality is much higher for the second Mg²⁺ ion (16.9%). This is accompanied by a higher flexibility for the second ion (*B* factor of 12.9 Å² compared with 8.2 Å² for the first ion). It is tempting to speculate that the first Mg²⁺ ion serves a structural role while the second Mg²⁺ ion contributes to enzymatic activity by acting as an electron sink. This notion is corroborated by docking experiments performed on human ARH3, in which the second Mg²⁺ ion coordinates the 2'-hydroxyl group of the ribose carrying the scissile glycosidic bond (Mueller-Dieckmann *et al.*, 2006).

3.3. Comparison with human ADP-ribosylhydrolase 3

A superposition of the two protomers of ARH3 from mouse with the structure of human ARH3 (PDB code 2foz) shows an r.m.s. deviation of only 0.40 Å for 336 superimposed C^α atoms for the first protomer and 0.52 Å for 331 superimposed C^α atoms for the second

protomer. Compared with the human ARH3 protein, there are a total of 26 substituted amino-acid residues, of which 17 can be described as conservative substitutions (Fig. 5). Table 4 lists all of the substitutions between mouse and human ARH3. All but two substitutions are located on the protein surface and do not alter the electrostatic surface potential. The two substitutions which are not located on the protein surface but in the protein core are Thr66 and Val233, which are Ala and Ile in the human orthologue, respectively. Both substitutions are far away from the active-site crevice. Thr66 is located on α -helix 3 and its closest distance to the Mg^{2+} ions is around 10 Å. It forms a hydrogen bond to the carbonyl O atom of Asp62 through its

hydroxyl group (2.8 Å), which is in turn involved in the Mg^{2+} coordination. The substitution of Ala by Thr increases the number of hydrogen bonds formed by the carbonyl O atom of Asp62 from three to four. A comparison with the human protein shows that the position of Asp62 is unaltered, suggesting that the substitution has no effect on the activity of the protein. Val233, on the other hand, is located around 19 Å away from the active site on α -helix 12 at the hydrophobic interface with α -helix 14. The substitution of Ile by Val leaves a hole at the position of the missing methyl group but presumably does not have an effect either on the stability of the protein or on the enzymatic activity. A comparison of the residues coordinating the two

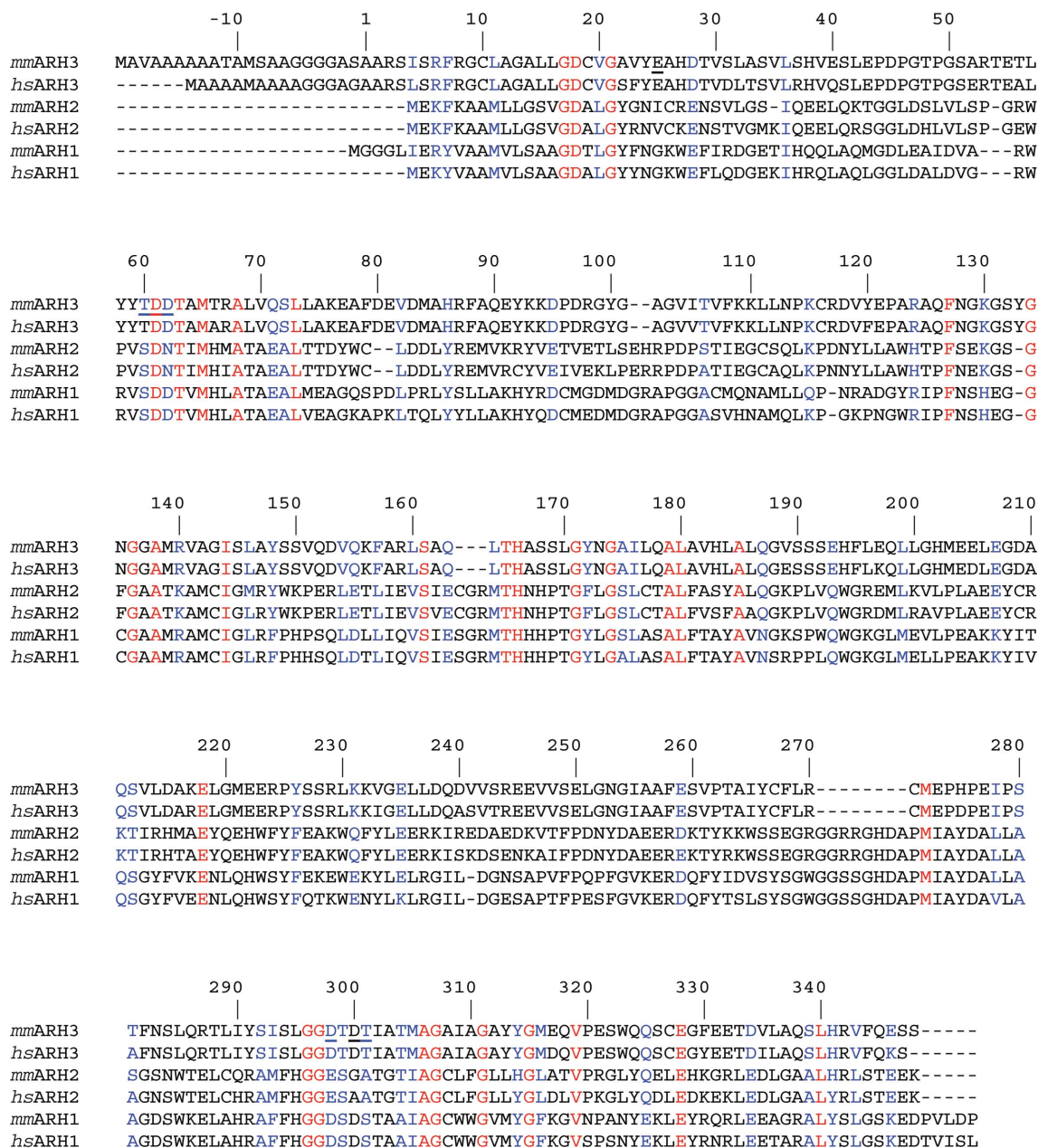


Figure 5 Sequence alignment of ARHs. All three ARH families from *M. musculus* (*mm*) and *Homo sapiens* (*hs*) were aligned using the program *ClustalW* (Chenna *et al.*, 2003); the numbering of residues is according to the mARH3 sequence in the crystal structure (2qty), *i.e.* without the mitochondrial targeting sequence. Identical residues are shown in red and similar residues are shown in blue. Residues that participate in the coordination of the two Mg^{2+} ions are underlined. Sequence identities within the family from *M. musculus* are 16.2% for mARH3 and mARH2, 17.4% for mARH3 and mARH1 and 42.1% for mARH1 and mARH2, while the sequence identity between mARH3 from *M. musculus* and *H. sapiens* is 89.7%.

Table 5Structural comparison of mARH3 using the search algorithms from *DALI* (Holm & Sander, 1996) and *SSM* (Krissinel & Henrick, 2004).Only results with a *Z* score higher than 2 are listed. The superposition of mARH3 with the corresponding protein was performed with the brute-force method implemented in the program *LSQMAN* (Novotny *et al.*, 2004), from which the number of superimposed amino-acid residues, r.m.s. deviation and r.m.s. ΔB factor values were taken.

Protein name	Organism	PDB code	Annotated function	Space group	Resolution (Å)	No. of amino-acid residues	No. of superimposed C α positions	<i>Z</i> score	R.m.s. deviation (Å)	R.m.s. ΔB factor (Å 2)	Reference†
ADP-ribosylhydrolase 3	<i>H. sapiens</i>	2g4k	De-ADP-ribosylation	<i>P</i> 2 ₁ 2 ₁ 2 ₁	1.82	336	336	63.3‡, 15.7§	0.47	14.5	<i>a</i>
ADP-ribosylhydrolase 3	<i>H. sapiens</i>	2fp0	De-ADP-ribosylation	<i>P</i> 2 ₁	2.05	335	335	15.9§	0.58	30.0	<i>b</i>
ADP-ribosylhydrolase 3	<i>H. sapiens</i>	2foz	De-ADP-ribosylation	<i>P</i> 2 ₁ 2 ₁ 2 ₁	1.60	336	336	15.9§	0.40	6.2	<i>b</i>
Ribosylglycohydrolase MJ1187	<i>Methanococcus jannaschii</i>	1t5j	Unknown	<i>P</i> 4 ₃ 2 ₁ 2	2.70	301	246	9.4§	1.36	34.1	<i>c</i>
ADP-ribosylglycohydrolase	<i>T. thermophilus</i> HB8	2cwc	De-ADP-ribosylation	<i>P</i> 2 ₁ 2 ₁ 2 ₁	1.65	303	240	8.5§	1.44	6.5	<i>d</i>
ADP-ribosylglycohydrolase	<i>T. thermophilus</i> HB8	2yzw	De-ADP-ribosylation	<i>P</i> 2 ₁ 2 ₁ 2 ₁	1.70	303	241	8.5§	1.30	6.8	<i>e</i>
ADP-ribosylglycohydrolase	<i>T. thermophilus</i> HB8	2yzv	De-ADP-ribosylation	<i>P</i> 2 ₁ 2 ₁ 2 ₁	1.60	303	241	8.4§	1.42	6.4	<i>e</i>
Methyl-coenzyme M reductase	<i>Methanobacterium thermoautotrophicum</i>	1mro	Methanogenesis	<i>P</i> 2 ₁	1.16	548	69	4.2‡	2.14	4.4	<i>f</i>
Hat domain of murine CstF-77	<i>Mus musculus</i>	2ooc	Polyadenylation of mRNA precursors	<i>H</i> 32	3.00	400	54	2.5‡	2.22	40.3	<i>g</i>

† (*a*) Mueller-Dieckmann *et al.* (2007); (*b*) Mueller-Dieckmann *et al.* (2006); (*c*) deposited in the PDB 11 May 2004; (*d*) deposited in the PDB 18 June 2005; (*e*) deposited in the PDB 6 November 2007; (*f*) Ermler *et al.* (1997); (*g*) Bai *et al.* (2007). ‡ Results from *DALI*. § Results from *SSM*.

Mg $^{2+}$ ions shows essentially no difference (the r.m.s. deviation is 0.11 Å for 55 atoms), which suggests that the active site is not altered between the two proteins. Likewise, those 14 residues that were identified in human ARH3 as being likely to participate in the binding of ADP-ribose (Glu25, Asp61, Gly103, Val104, Thr106, Asn126, Phe127, Ser132, Tyr133, Asn135, His166, Glu259, Asp298 and Thr301) have an r.m.s. deviation to the mouse orthologue of only 0.55 Å (for 115 atoms), implying that the binding mode is essentially the same in those two proteins.

3.4. Comparison of the structural fold of mARH3 to prokaryotic homologues

A protein structure comparison of mARH3 with proteins deposited in the PDB using *DALI* (Holm & Sander, 1996) and *SSM* (Krissinel & Henrick, 2004) gave the structure of the human orthologue with the highest *Z* score for both search algorithms (see §3.3 and Table 5). In addition, two prokaryotic proteins (PDB codes 1t5j from the archaeon *Methanococcus jannaschii* and 2cwc from the Gram-negative eubacterium *Thermus thermophilus*), as well as two metal complexes of 2cwc (2yzv and 2yzw), were identified using the program *SSM* with *Z* scores of 9.4, 8.5 and 8.4, respectively. Like mARH3, they are all α -helical proteins and show a high degree of structural similarity (82% and 79% of all amino-acid residues can be superimposed with an r.m.s. deviation of 1.4 Å for 246 C α positions for 1t5j and 240 C α positions for 2cwc; Table 5). The proposed active-site crevice shows a high degree of agreement of the positions of the α -helices and loop structures that form this crevice. However, there are also two notable differences in terms of the apparent accessibility to this crevice. An additional α -helix (helix 2) that is present in mouse ARH3 (as well as the human protein) but not in the prokaryotic proteins seems to block access to the active site from this side. The other difference concerns the 'missing loop' region (Asp45–Thr54) in mouse ARH3 (and its human orthologue). The corresponding region in 1t5j and 2cwc folds back and forms a kind of lid that blocks access from this side of the active site. To gain full accessibility to the two Mg $^{2+}$ ions, this lid would need to move away. In the case of 1t5j at least, there is one residue within this lid (Tyr49) that participates in a hydrogen-bonding network together with other Mg $^{2+}$ -coordinating residues.

The data for 2cwc and its two metal-ion-containing analogues 2yzv and 2yzw were all collected by the RIKEN structural genomics/

proteomics initiative at SPring-8 in Japan at a wavelength of 1.0 Å to rather high resolutions of 1.65 Å (2cwc), 1.60 Å (2yzv) and 1.70 Å (2yzw). The structures of 2yzv, which contains two Mg $^{2+}$ ions, and of 2yzw, which contains two Gd $^{3+}$ ions, superimpose very well on each other with an r.m.s. deviation of 0.16 Å for 283 superimposed C α atoms, as well as with 2cwc with an r.m.s. deviations of 0.24 Å for 284 superimposed C α atoms for 2yzv and 0.26 Å for 282 superimposed C α atoms for 2yzw. The two Mg $^{2+}$ ions within the 2yzv structure are 3.5 Å apart from each other. The first Mg $^{2+}$ ion, with a *B* factor of 18 Å 2 , is coordinated by one Thr and two Asp residues (both coordinating bidentally), while the second ion has a higher *B* factor of 30 Å 2 and is coordinated by one Thr and three Asp residues (one coordinating bidentally). Both ions are not octahedrally coordinated because there are no coordinating water molecules. A comparison with the 2cwc structure shows little structural difference for the three coordinating residues for the first Mg $^{2+}$ ion, while for the second Mg $^{2+}$ ion two of the three coordinating Asp residues have shifted by 3.4 and 6.3 Å. Compared with mouse ARH3, there is hardly any difference in the coordination of the first Mg $^{2+}$ ion, although Glu25 in the ARH3 structure is within coordination distance of this ion. The second Mg $^{2+}$ ion also shows good agreement compared with ARH3, with the exception that one Asp residue has moved by 1.9 Å.

The situation is similar for 2yzw, which contains two Gd $^{3+}$ ions 3.76 Å apart from each other with comparable *B* factors of 13 and 16 Å 2 . Although the maximal resolution of this structure is somewhat lower than that of 2yzv, both ions are roughly octahedrally coordinated. The first Gd $^{3+}$ ion is coordinated by two water molecules (of which one is a bridging water molecule between the two metal ions), one Thr, one Glu and two Asp residues (one Asp residue coordinates to both metal ions) and the second Gd $^{3+}$ ion is coordinated by one Thr and three Asp residues as well as two water molecules. A comparison with the structure of 2cwc shows a large movement of the Glu residue (by 1.8 Å) for the first Gd $^{3+}$ ion and also a large movement of two of the three coordinating Asp residues. Compared with the mouse ARH3 structure, there is hardly any movement within the coordinating residues of both metal ions apart from a 0.9 Å movement of the coordinating Glu residue.

Using the search algorithm from the program *DALI* a (weak) structural similarity (*Z* scores of 4.2 and 2.4, respectively) was detected to two bacterial enzymes (PDB codes 1mro and 2ooc), one of which is involved in bacterial methanogenesis and the other in polyadenylation of mRNA precursors. Given the fact that only 68 out

of 548 amino-acid residues can be superimposed with an r.m.s. deviation of 2.06 Å for 1mro (Ermler *et al.*, 1997) and 54 out of 400 amino-acid residues with an r.m.s. deviation of 2.22 Å for 2ooe (Bai *et al.*, 2007), it is clear that these proteins do not share a common fold with mARH3.

4. Summary and conclusion

We have determined the three-dimensional crystal structure of murine ADP-ribosylhydrolase 3 to 1.8 Å resolution. The structure constitutes a compact all- α -helical protein with two Mg²⁺ ions that pinpoint the active-site crevice. A comparison with the recently published structure of the human orthologue (Mueller-Dieckmann *et al.*, 2006) shows a high degree of structural consistency; similar observations were made using the three-dimensional structures of four prokaryotic proteins deposited in the PDB.

Parts of the work described in this study represent partial fulfilment of the requirements for the doctoral thesis of SK at the University of Hamburg. This work was supported by grants from the Deutsche Forschungsgemeinschaft (to FK-N and MSW) and the Studienstiftung des deutschen Volkes (to SK).

References

- Ahuja, N., Schwer, B., Carobbio, S., Waltregny, D., North, B. J., Castronovo, V., Maechler, P. & Verdin, E. (2007). *J. Biol. Chem.* **282**, 33583–33592.
- Aktories, K. & Just, I. (2000). *Bacterial Protein Toxins*. Berlin: Springer-Verlag.
- Bai, Y., Auperin, T. C., Chou, C.-Y., Chang, G.-G., Manley, J. L. & Tong, L. (2007). *Mol. Cell.* **25**, 863–875.
- Chang, P., Jacobson, M. K. & Mitchison, T. J. (2004). *Nature (London)*, **432**, 645–649.
- Chenna, R., Sugawara, H., Koike, T., Lopez, R., Gibson, T. J., Higgins, D. G. & Thompson, J. D. (2003). *Nucleic Acids Res.* **31**, 3497–3500.
- Collaborative Computational Project, Number 4 (1994). *Acta Cryst.* **D50**, 760–763.
- Emsley, P. & Cowtan, K. (2004). *Acta Cryst.* **D60**, 2126–2132.
- Ermler, U., Grabarse, W., Shima, S., Goubeaud, M. & Thauer, R. K. (1997). *Science*, **278**, 1457–1462.
- French, S. & Wilson, K. (1978). *Acta Cryst.* **A34**, 517–525.
- Glowacki, G., Braren, R., Firner, K., Nissen, M., Kuehl, M., Reche, P., Bazan, F., Cetkovic Cvrlje, M., Leiter, E., Haag, F. & Koch-Nolte, F. (2002). *Protein Sci.* **11**, 1657–1670.
- Haigis, M. C., Mostoslavsky, R., Haigis, K. M., Fahie, K., Christodoulou, D. C., Murphy, A. J., Valenzuela, D. M., Yancopoulos, G. D., Karow, M., Blander, G., Wolberger, C., Prolla, T. A., Weindruch, R., Alt, F. W. & Guarente, L. (2006). *Cell*, **126**, 941–954.
- Harding, M. M. (2001). *Acta Cryst.* **D57**, 401–411.
- Harding, M. M. (2006). *Acta Cryst.* **D62**, 678–682.
- Hassa, P. O., Haenni, S. S., Elser, M. & Hottiger, M. O. (2006). *Microbiol. Mol. Biol.* **70**, 789–829.
- Holm, L. & Sander, C. (1996). *Science*, **273**, 595–603.
- Jagtap, P. & Szabo, C. (2005). *Nature Rev. Drug Discov.* **4**, 421–440.
- Kernstock, S., Koch-Nolte, F., Mueller-Dieckmann, J., Weiss, M. S. & Mueller-Dieckmann, C. (2006). *Acta Cryst.* **F62**, 224–227.
- Kim, M. Y., Mauro, S., Gevrey, N., Lis, J. T. & Kraus, W. L. (2004). *Cell*, **119**, 803–814.
- Koch-Nolte, F. & Haag, F. (1997). *Adv. Exp. Med. Biol.* **419**, 1–13.
- Krissinel, E. & Henrick, K. (2004). *Acta Cryst.* **D60**, 2256–2268.
- Lennon, G. G., Auffray, C., Polymeropoulos, M. & Soares, M. B. (1996). *Genomics*, **33**, 151–152.
- Malanga, M. & Althaus, F. R. (2005). *Biochem. Cell. Biol.* **83**, 354–364.
- Meyer, R. G., Meyer-Ficca, M. L., Whatcott, C. J., Jacobson, E. L. & Jacobson, M. K. (2007). *Exp. Cell Res.* **313**, 2920–2936.
- Morrison, A. R., Moss, J., Stevens, L. A., Farrell, C., Merithew, E., Lambright, D. G., Greiner, D. L., Mordes, J. P., Rossini, A. A. & Bortell, R. (2006). *J. Biol. Chem.* **281**, 33363–33372.
- Moss, J., Jacobson, M. K. & Stanley, S. J. (1985). *Proc. Natl Acad. Sci. USA*, **82**, 5603–5607.
- Moss, J., Zolkiewska, A. & Okazaki, I. (1997). *Adv. Exp. Med. Biol.* **419**, 25–33.
- Mueller-Dieckmann, C., Kernstock, S., Lisurek, M., von Kries, J.-P., Haag, F., Weiss, M. S. & Koch-Nolte, F. (2006). *Proc. Natl Acad. Sci. USA*, **103**, 15026–15031.
- Mueller-Dieckmann, C., Panjekar, S., Schmidt, A., Mueller, S., Kuper, J., Geerlof, A., Wilmanns, M., Singh, R. K., Tucker, P. A. & Weiss, M. S. (2007). *Acta Cryst.* **D63**, 366–380.
- Mueller-Dieckmann, J. (2006). *Acta Cryst.* **D62**, 1446–1452.
- Niere, M., Kernstock, S., Koch-Nolte, F. & Ziegler, M. (2008). *Mol. Cell. Biol.* **28**, 814–824.
- Novotny, M., Madsen, D. & Kleywegt, G. J. (2004). *Proteins*, **54**, 260–270.
- Oka, S., Kato, J. & Moss, J. (2006). *J. Biol. Chem.* **281**, 705–713.
- Ono, T., Kasamatsu, A., Oka, S. & Moss, J. (2006). *Proc. Natl Acad. Sci. USA*, **103**, 16687–16691.
- Otto, H., Reche, P. A., Bazan, F., Dittmar, K., Haag, F. & Koch-Nolte, F. (2005). *BMC Genomics*, **6**, 139–161.
- Otwinowski, Z. & Minor, W. (1997). *Methods Enzymol.* **276**, 307–326.
- Schreiber, V., Dantzer, F., Ame, J. C. & de Murcia, G. (2006). *Nature Rev. Mol. Cell Biol.* **7**, 517–528.
- Seman, M., Adriouch, S., Haag, F. & Koch-Nolte, F. (2004). *Curr. Med. Chem.* **11**, 857–872.
- Shall, S. (1995). *Biochimie*, **77**, 313–318.
- Smith, S., Giriat, I., Schmitt, A. & de Lange, T. (1998). *Science*, **282**, 1484–1487.
- Vagin, A. & Teplyakov, A. (1997). *J. Appl. Cryst.* **30**, 1022–1025.
- Weiss, M. S. (2001). *J. Appl. Cryst.* **34**, 130–135.
- Winn, M. D., Isupov, M. N. & Murshudov, G. N. (2001). *Acta Cryst.* **D57**, 122–133.
- Yu, W., Ginja, V., Pant, V., Chernukhin, I., Whitehead, J., Docquier, F., Farrar, D., Tavosidana, G., Mukhopadhyay, R., Kanduri, C., Oshimura, M., Feinberg, A. P., Lobanenko, V., Klenova, E. & Ohlsson, R. (2004). *Nature Genet.* **36**, 1105–1110.